Room-temperature autonomous self-healing glassy polymers with hyperbranched structure

Hao Wang[a], Hanchao Liu[a], Zhenxing Cao[a], Weihang Li[a], Xin Huang[a], Yong Zhu[a], Fangwei Ling[a], Hu Xu[a], Qi Wu[a], Yan Peng[a], Bin Yang[b], Rui Zhang[c], Olaf Kessler[b], Guangsu Huang[a], and Jinrong Wu[a,1]

[a]State Key Laboratory of Polymer Materials Engineering, College of Polymer Science and Engineering, Sichuan University, 610065 Chengdu, China; [b]°CALOR-Competence Center Calorimetry and Thermal Analysis Rostock, Materials Science, University of Rostock, 18051 Rostock, Germany; and [c]Institute of Physics, University of Rostock, 18051 Rostock, Germany

Edited by Frank S. Bates, University of Minnesota, Minneapolis, MN, and approved April 6, 2020 (received for review January 1, 2020)

Glassy polymers are extremely difficult to self-heal below their glass transition temperature (T_g) due to the frozen molecules. Here, we fabricate a series of randomly hyperbranched polymers (RHP) with high density of multiple hydrogen bonds, which show T_g up to 49 °C and storage modulus up to 2.7 GPa. We reveal that the hyperbranched structure not only allows the external branch units and terminals of the molecules to have a high degree of mobility in the glassy state, but also leads to the coexistence of "free" and associated complementary moieties of hydrogen bonds. The free complementary moieties can exchange with the associated hydrogen bonds, enabling network reconfiguration in the glassy polymer. As a result, the RHP shows amazing instantaneous self-healing with recovered tensile strength up to 5.5 MPa within 1 min, and the self-healing efficiency increases with contacting time at room temperature without the intervention of external stimuli.

glassy polymers | self-healing | randomly hyperbranched polymers | hydrogen bond

Intrinsic self-healing polymers are materials capable of repairing mechanical damage through reversible bonding between molecular chains (1–5). As such, intrinsic self-healing can be repeated multiple times (6–8), which is superior to extrinsic self-healing relying on preembedded healing agents (9, 10). The reversible bonding generally includes supramolecular interactions such as hydrogen bonds (7, 11–13), host–guest interactions (14, 15), metal–ligand coordination (16–19) and ionic interactions (20–22), and reversible covalent bonds such as Diels–Alder reactions (6, 23), imine bond (24, 25), disulfide bond (26, 27), dynamic urea bond (28), and boron ester bond (29–31). Healing through both types of reversible bonding is actually a physical–chemical process, in which the cleaved moieties need to find their counterparts to reform enthalpically favorable bonds, while the chain segments experience conformational changes and diffusion to reach a new equilibrium state. This physical–chemical process requires high molecular mobility to accomplish, thus intrinsic self-healing under room temperature is usually reported in elastomers and hydrogels (1, 12–14, 19–21, 27, 32). However, polymers with glass transition temperature (T_g) higher than room temperature need thermal stimulus (33, 34) or solvent assistance (25, 35, 36) to heal, which are nevertheless inaccessible during most practical applications. To date, it remains a huge challenge to fabricate stiff glassy polymers with self-healing ability at room temperature.

Glassy polymers show high mechanical modulus and strength, and thus are widely used as structural materials in aerospace vehicles, airplanes, automobiles, biomedical devices, and so on. The high mechanical properties of glassy polymers are closely related to their frozen network under room temperature. However, under such state the mobility of polymer chains is severely restricted. Therefore, the freshly fractured sections of the materials are difficult to recombine together, i.e., the diffusion of molecules across the sections are limited and the cleaved moieties cannot reform reversible bonds. Thus, self-healing cannot take place below T_g. To address this issue, Aida and coworkers synthesized a class of poly(ether-thioureas) with a large number of nonlinear zigzag arrays of H-bonded thiourea units (37). Although the polymer is amorphous and has a T_g above room temperature, its self-healing at room temperature can be achieved through the slip of hydrogen bonds between molecular chains under the intervention of external compression force. While this seminal work points out that self-healing below T_g is feasible for polymers, a dire shortage of alternative strategies has severely limited the scope of glassy polymers with room-temperature malleability.

Hyperbranched polymers differ from traditional linear polymers. They have three-dimensional spatial molecular configuration: unique internal structure and abundant external branching units and end groups. Usually, the internal segments are highly jammed and thus have low molecular mobility, while the external branch units and end groups possess a high degree of mobility (38, 39). Thus, we can envision that a glassy hyperbranched polymer may manifest mobile external branch units and end groups, on which if we elaborately introduce the self-healing complementary moieties, the hyperbranched polymers may have room-temperature self-healing ability. As a proof of concept, we fabricated a class of randomly hyperbranched polymers (RHP) bearing not only primary amine terminals, but also amide groups and secondary amines on branched chains. These complementary moieties are able to form multiple hydrogen bonds with high density; thus, RHP is a glassy polymer

Significance

Glassy polymers are widely used as structural materials in aerospace vehicles, airplanes, automobiles, biomedical devices, and so on. However, glassy polymers are difficult to self-heal at room temperature due to their frozen molecules. For example, the window glass of airplanes made of polycarbonate cannot repair mechanical damages autonomously, which could lead to a catastrophe. To impart glassy polymers with self-healing ability, we take advantage of the high mobility of hyperbranched polymers, and introduce hydrogen complementary moieties onto the hyperbranched structure, enabling the construction of a series of autonomous room-temperature self-healing glassy polymers.

Author contributions: H.W. and J.W. designed research; H.W. performed research; B.Y., R.Z., and O.K. contributed new reagents/analytic tools; H.W., H.L., Z.C., W.L., X.H., Y.Z., F.L., H.X., Q.W., Y.P., and G.H. analyzed data; H.W. wrote the paper; Q.W., Y.P., B.Y., and R.Z. assisted with the characterization; O.K. and G.H. assisted with the paper writing; and J.W. conceived the concept.

The authors declare no competing interest.

This article is a PNAS Direct Submission.

[1]To whom correspondence may be addressed. Email: wujinrong@scu.edu.cn.

This article contains supporting information online at https://www.pnas.org/lookup/suppl/doi:10.1073/pnas.2000001117/-/DCSupplemental.

First published May 7, 2020.

with T_g up to 49 °C, tensile strength up to 18.5 MPa, and storage modulus up to 2.7 GPa at room temperature. We reveal that the branch units and end groups are highly mobile even in the glassy state. Moreover, the randomly branched structure of RHP prevents the ordered packing of the molecules, so that a part of the complementary moieties cannot find their counterparts to form hydrogen bonds. Due to the mobility of the external structure, these "free" moieties can exchange with the associated hydrogen bonds, leading to the reconfiguration of the network structure. As a result, the fractured RHP can amazingly recover a tensile strength of 5.5 MPa within 1 min, and the recovered tensile strength increases continuously at room temperature without the assistance of external force.

Results and Discussion

We synthesized a series of RHP by one-pot Michael addition between *N,N'*-methylene diacrylamide (MBA) and 1,4-butanediamine (BDA) at different molar ratios (Fig. 1*A*). The schematic diagram of synthetic reaction mechanism is shown in *SI Appendix*, Fig. S1. The reaction was carried out under mild conditions (30 °C, 24 h) with quite high conversion ratio (up to 92.1%) (*SI Appendix*, Table S1). The Michael addition results in tertiary and secondary amines, which serve as branching points and chain-extending units, respectively. Because each -NH- of BDA can react with a CH_2 = CH- on MBA and the mole ratio between -NH- and CH_2 = CH- is from 9/4 to 7/4, the RHP molecules are terminated with primary amine. We synthesize three RHP materials denoted as RHP-1, RHP-2, and RHP-3, corresponding to MBA/BDA molar ratios of 1/1.125, 1/1, and 1/0.875, respectively. When the MBA/BDA molar ratio exceeds 1/0.875, gelation takes place quickly during the Michael addition (*SI Appendix*, Fig. S2), resulting in permanent covalent networks, which is undesirable for self-healing polymers.

The molecular structure of RHP was examined by Fourier transformation infrared spectroscopy (FTIR) and ^{1}H NMR. The results confirm the formation of the RHP molecules through Michael addition reaction between MBA and BDA (*SI Appendix*, Fig. S3). Moreover, it is revealed that the different MBA/BDA molar ratio leads to different percentage of primary amine, secondary amine, and tertiary amine units in each RHP (*SI Appendix*, Fig. S4). Specifically, as the molar ratio between MBA and BDA increases from 1/1.125 to 1/0.875, the percentage of primary amine units decreases from 22.8 to 14.6% while that of tertiary amine units increases from 13.4 to 30.8% (*SI Appendix*, Table S2). Such phenomenon is attributed to the increased proportion of CH_2 = CH- at high MBA/BDA molar ratio, which further consumes the primary and secondary amines on RHP, leading to a gradual increase in the molecular weight (details shown in *SI Appendix*, Table S3). Moreover, we used dynamic light scattering to demonstrate the molecular size of RHP. The molecular size of RHP increases with MBA/BDA ratio (*SI Appendix*, Fig. S5 and Table S3). Meanwhile, the degree of branching (DB) also increases, due to the increased fraction of tertiary amine. The DB value can be calculated by ^{13}C, ^{1}H-heteronuclear single quantum correlation and quantitative ^{13}C NMR spectra (*SI Appendix*, Fig. S6 and Table S4). The results show that the DB value increase from 0.16 of RHP-1 to 0.33 of RHP-3.

Since each MBA unit has two amide groups which can form hydrogen bonds with other amide groups and secondary and primary amines (Fig. 1*C*), the density of hydrogen bonds is very high in the RHP networks, which leads to high T_g of the materials. Fig. 1*B* illustrates a schematic diagram of interactions between RHP molecules. To examine the thermodynamic properties of the RHP materials, differential scanning calorimetry (DSC) measurements were carried out (Fig. 2*A* and

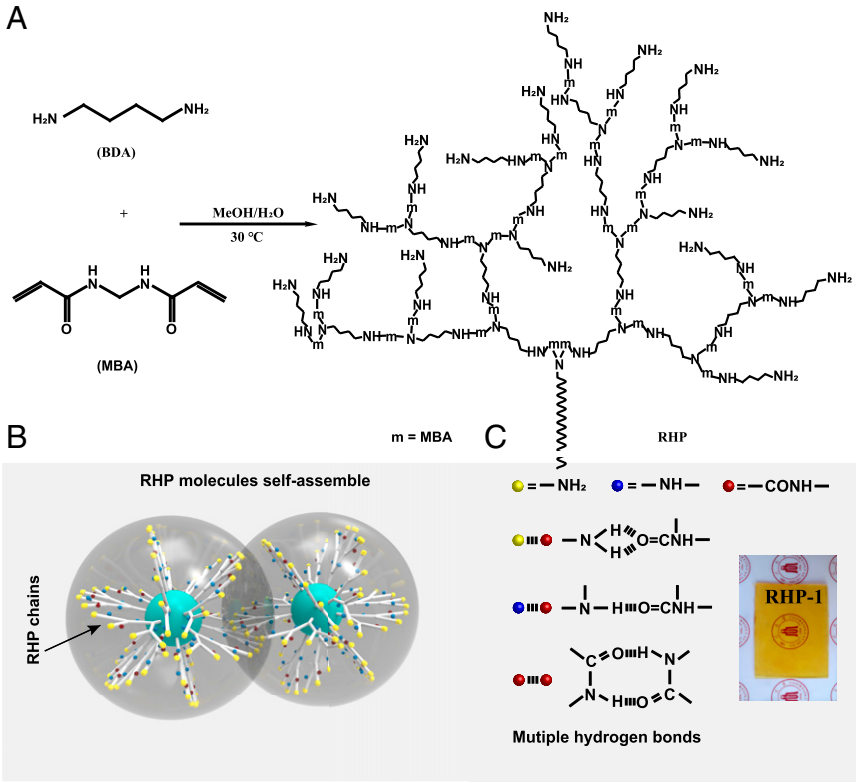

Fig. 1. Design concept and synthesis of RHP. (*A*) Chemical route to the synthesis of RHP through Michael addition between MBA and BDA at 30 °C (the reaction details are shown in *SI Appendix*, Fig. S1). (*B*) Schematic diagram of interactions between RHP molecules. (*C*) Multiple hydrogen bonds of RHP molecules. (*Inset*) A photograph of RHP-1.

SI Appendix, Table S3). It is revealed that the T_g values of RHP-1, RHP-2, and RHP-3 are 37, 42, and 49 °C, respectively, suggesting that they are glassy polymers at room temperature. The increase in T_g with the increasing molar ratio between MBA and BDA can be attributed to the larger molecular size and less terminal groups of RHP-2 and RHP-3. Notably, RHP-1 shows a high melting point at 122 °C, indicating that there are crystals in the materials (*SI Appendix*, Fig. S7). X-ray diffraction (XRD) measurements show sharp crystallization peaks in RHP-1, while only a broad peak can be observed in RHP-2 and RHP-3 (Fig. 2*B*). Therefore, RHP-1 is semicrystalline, and RHP-2 and RHP-3 are amorphous. The crystallization of RHP-1 is closely related to the lower degree of branching and smaller molecular size, which facilitate the ordered arrangement of the molecules (40). Dynamic mechanical analysis demonstrates that RHP-1 has the highest storage modulus of 2,721 MPa at 25 °C (Fig. 2 *C* and *D*), due to the reinforcement effect of crystals. Meanwhile, RHP-3 shows higher storage modulus than RHP-2 at 25 °C, suggesting that increasing the molecular size and decreasing the number of terminals can improve the stiffness of the materials. Despite the difference, the high storage modulus from 1,616 to 2,721 MPa is comparable to that of most glassy polymers at room temperature (41–43). Moreover, the transition from glassy state to rubbery state takes place well above 25 °C (Fig. 2*C*), which further confirms that the obtained materials are in the glassy state at room temperature.

To study the molecular dynamics of the RHP materials, broadband dielectric spectrum measurements were performed. We artificially divide the dielectric relaxation into two regimes: above T_g and below T_g, because the modes of molecular motion of RHP are different in these regimes. Above T_g, due to the presence of strong direct current (DC) conductivity, the dielectric permittivity and loss of RHP are masked. Hence, we need another strategy called the dielectric modulus formalism to distinguish the relaxation process; see details in *SI Appendix* (44). The dielectric loss modulus spectra show an obvious relaxation process (*SI Appendix*, Fig. S8*A*), which is assigned to the structural α-relaxation (segmental motion). The average relaxation time τ of the α-process obtained from the frequency of maximum loss modulus is plotted as a function of temperature, which can be fitted by Vogel–Fulcher–Tammann (VFT) equation, as shown in Fig. 3*C* and *SI Appendix*. By extrapolating the VFT equation to 25 °C, we find that the average relaxation time of α-process is in the range from 10^5 s (RHP-1) to 10^9 s (RHP-3), as shown in *SI Appendix*, Table S5. This result demonstrates that the segmental motion can hardly take place around room temperature and thus the material can maintain its structural stability in glassy state. This result also reveals that the segmental motion does not contribute to the self-healing process at room temperature.

Below T_g, all dielectric loss spectra of RHP as a function of frequency show three relaxation processes, as shown in Fig. 3 *A* and *B* and *SI Appendix*, Fig. S8*B*. The three processes include β-relaxation (the local fluctuations of branch chains that include amino terminals), γ-relaxation (the motions of free amide groups), and δ-relaxation (the motion of surface terminal amino groups) (38). To quantitatively analyze these relaxation processes, we use a combination of three Havriliak–Negami (HN) functions (*SI Appendix*) and a conductivity term to fit the dielectric loss spectra (Fig. 3*B*). Average relaxation time of β-, γ-, and δ-processes of RHP can be extracted from the HN equations and plotted as a function of temperature, as shown in Fig. 3*C*. We can see that the δ-relaxation is fastest, followed by the γ-process and β process. Moreover, all these three relaxation modes can take place below T_g. These results prove our assumptions that the external branch chains, functional units, and terminals of RHP are mobile in the glassy state. Moreover, the relationship between the average relaxation time and temperature can be described by Arrhenius equation (*SI Appendix*), and the activation energies (E_a) are shown in Fig. 3*D*. It is clear that the E_a values of β-, γ-, and δ-processes are quite low (in the range from 15 to 71 kJ/mol). This is why these relaxation modes can easily take place in the glass state, which is critical to the self-healing process below T_g.

The occurrence of β-, γ-, and δ-processes can lead to the reorganization of hydrogen bonds. To characterize multiple hydrogen-bonding interactions of RHP, temperature-dependent

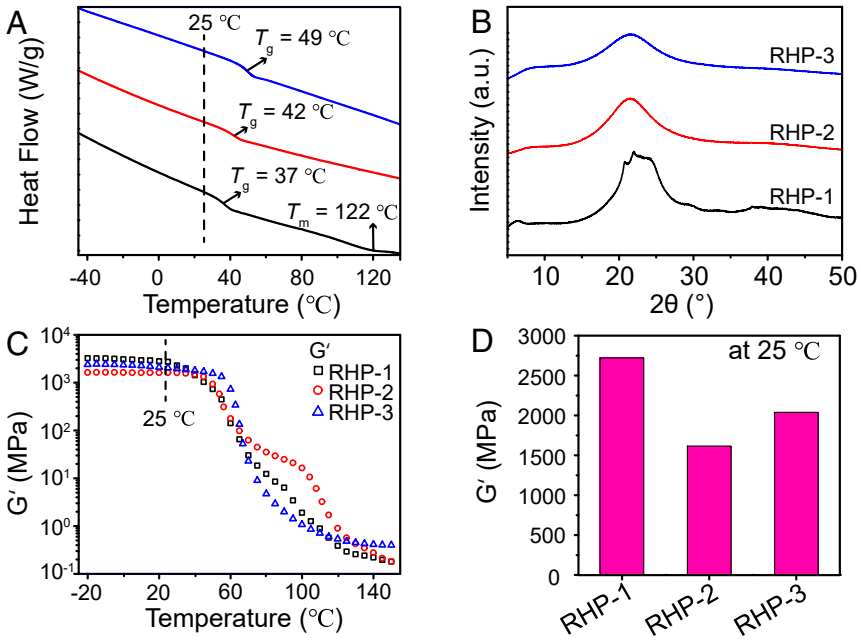

Fig. 2. Thermomechanical properties of RHP. (*A*) DSC thermograms for RHP on the second heating from −50 to 150 °C at a rate of 10 °C/min. From down to up, the samples are RHP-1, RHP-2, and RHP-3, respectively. (*B*) XRD profiles for RHP-1, RHP-2, and RHP-3 at 25 °C. (*C*) Temperature dependence of storage modulus of RHP and (*D*) storage modulus of RHP at 25 °C.

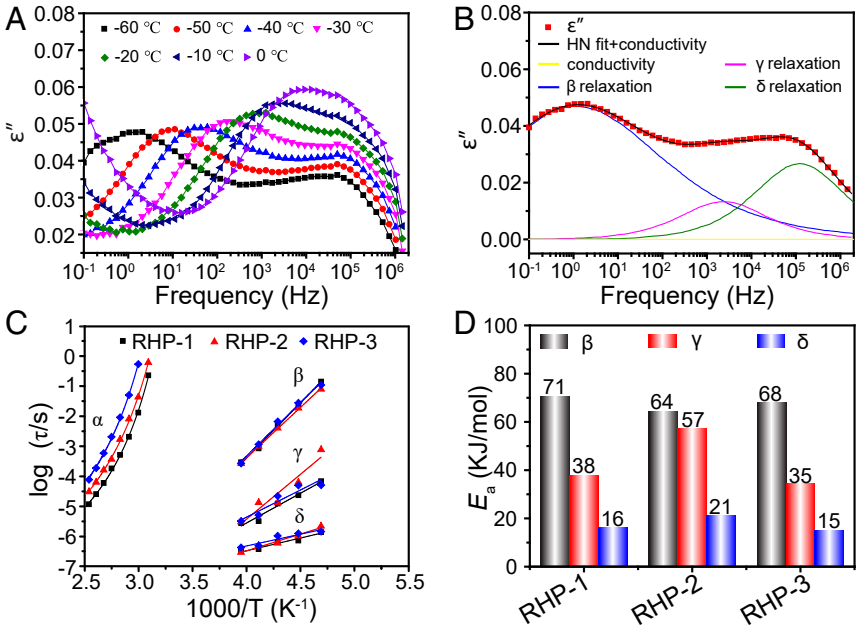

Fig. 3. Fig. 3 Dielectric relaxation behavior of RHP. (*A*) Dielectric loss ε'' as a function of frequency for RHP-1 from −60 to 0 °C. (*B*) Dielectric loss spectra of RHP-1 fitted by using a combination of three HN equations with DC conductivity at −60 °C. (*C*) Average relaxation time as a function of temperature for all relaxation processes in RHP. Solid lines represent VFT fitting for α-relaxation and Arrhenius fitting for other relaxation processes, respectively. (*D*) Activation energies (E_a) of RHP for β-, γ-, and δ-relaxation.

FTIR measurement was performed. Obviously, there are two peaks centered at 1,640 and 1,544 cm^{-1} at room temperature, belonging to the hydrogen-bonded amide I band and -NH- bending, respectively, as shown in Fig. 4*A* and *SI Appendix*, Fig. S9*A*. Moreover, these two peaks are very broad, indicating the coexistence of multiple hydrogen bonds and free amide and -NH- groups in the RHP molecules. As the temperature increases from 25 to 150 °C, the intensity around 1,640 cm^{-1} and 1,544 cm^{-1} decreases, while the intensity around 1,659 cm^{-1} (free amide groups) and 1,530 cm^{-1} (free -NH- groups) increases remarkably. The results prove that with the temperature increases, the associated hydrogen bonds gradually become dissociated (45). Temperature-dependent ^1H NMR was used to further study the hydrogen bonding interactions. The -NH- in the amide groups (8.58 ppm), the methylene beside -NH_2 (2.50 ppm, superimposed with dimethyl sulfoxide), and the methylene beside -NH- (2.65 ppm, the methylene of MBA attached to secondary amine after Michael addition; 2.44 ppm, the methylene of BDA attached to secondary amine after Michael addition) are clearly identified at 25 °C (Fig. 4 *B* and *C* and *SI Appendix*, Fig. S9*B*). As the temperature increases, the proton peak of -NH- in the amide groups shows an upfield shift and meanwhile the proton peak of methylene beside -NH_2 and -NH- shows a downfield shift. Such shifts are observed to begin at 25 °C, indicating that a part of the hydrogen bonds is already very dynamic at room temperature (46), which will facilitate the self-healing under this condition.

To further study the network dynamics around T_g of RHP, two-dimensional (2D) correlation analysis of -NH- vibration on FTIR spectra from 20 to 40 °C was performed, and the synchronous and asynchronous maps are shown in Fig. 4 *D* and *E*, respectively. The details of the sequential order of group mobility can be judged by Noda's rule in the 2D maps (*SI Appendix*) (47). In Fig. 4*D*, two autopeaks at [1,500, 1,500 cm^{-1}] and [1,510, 1,510 cm^{-1}] can be clearly identified in the synchronous map, corresponding to the bending vibration peaks of the different free -NH- moieties. The other two autopeaks at [1,541, 1,541 cm^{-1}] and [1,558, 1,558 cm^{-1}] are attributed to the different hydrogen-bonded -NH- moieties (48, 49). Compared with the region of hydrogen-bond moieties, the region of free -NH- moieties is more obvious, indicating that the free amino and amide groups have stronger motility in this temperature range. From the asynchronous map (Fig. 4*E*), two positive peaks at [1,558, 1,510 cm^{-1}] and [1,541, 1,510 cm^{-1}] are observed at the off-diagonal positions. According to the rule of 2D analysis, the peak at 1,510 cm^{-1} changes first, indicating that the free -NH- moieties start to move first and then exchange with the moieties from associated hydrogen bonds around room temperature; the schematic illustration is shown in Fig. 4*F*.

Due to the exchange of hydrogen bonds in the glassy state, the dynamic network can be reconfigurated, enabling self-healing of RHP. The self-healing behavior is visually demonstrated in Fig. 5*A* and Movie S1. A RHP-1 rectangle sheet of 30 × 10 × 1 mm^3 is broken into two pieces, and the pieces are brought into contact immediately. The sheet can bear a weight of 300 g after 1 min. To quantitatively examine the self-healing efficiency of RHP, the dumbbell-shaped specimens were cut and then rejointed to allow healing for different time periods at 25 °C. Stress–strain curves of the mended samples were acquired by uniaxial tensile tests with a strain rate of 10 mm/min and compared with that of the virgin sample (Fig. 5*B* and *SI Appendix*, Fig. S10). Remarkably, RHP can recover a tensile stress up to 5.5 MPa after the fractured pieces are contacted for 1 min, as shown in *SI Appendix*, Fig. S8. Such outstanding instantaneous self-healing with high-recover tensile stress is superior to most self-healing materials (Fig. 5*C*) (50–56). It is closely related to the high mobility of the branched chains and terminals, a unique feature of RHP, which allows the quick reformation of hydrogen bonds across the fractured surface through dissociated moieties. As the molecular size increases, the number of terminals of RHP decreases, and thus the molecular mobility becomes slower. As a result, the instantaneous self-healing efficiency decreases from 33.4% of RHP-1 to 27.2% of RHP-3. However, as the contact time prolongs, the self-healing efficiency can be improved

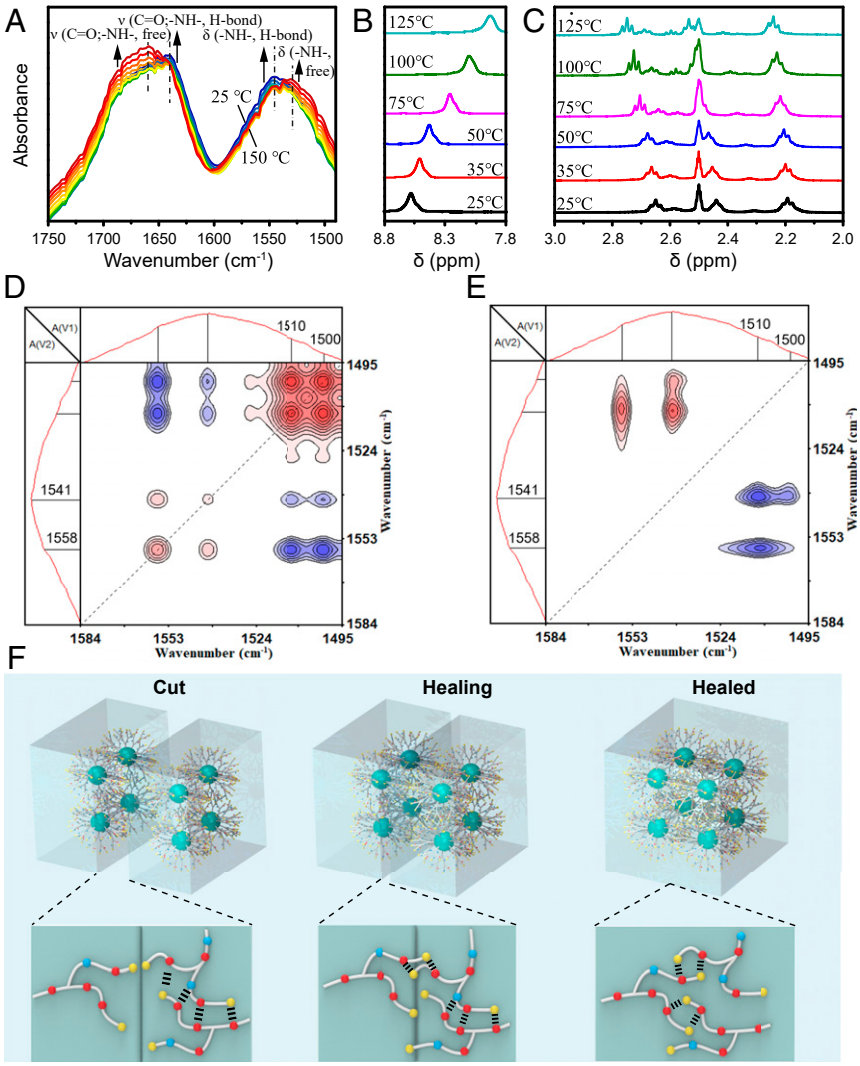

Fig. 4. Multiple hydrogen bonds and self-healing mechanism of RHP. (*A*) Temperature-dependent FTIR spectra of RHP upon heating from 25 to 150 °C. (*B* and *C*) ^{1}H NMR spectral change of RHP-1 in deuterated dimethyl sulfoxide with an increase in temperature from 25 to 125 °C (from down to up, the temperatures are 25, 35, 50, 75, 100, and 125 °C, respectively): (*B*) 7.8–8.8 ppm; (*C*) 2.0–3.0 ppm. Synchronous (*D*) and asynchronous (*E*) maps of the RHP-1 in the region 1,585–1,495 cm^{-1} during the heating process from 20 to 40 °C. (*F*) Schematic illustration of the self-healing process of RHP showing the free moieties moving first and then exchanging with the associated hydrogen bonds (yellow, blue, and red circles represent the primary amine, secondary amine, and amide groups, respectively).

significantly. When the samples are mended for 48 h, the self-healing efficiencies of RHP-1, RHP-2, and RHP-3 increase to 75.56, 67.63, and 59.35%, respectively. Such results indicate that the branched chains are able to interpenetrate across the fractured surface to form more hydrogen bonds given enough time, leading to the improvement of self-healing efficiency.

Conclusions

In summary, this work provides a strategy and mechanism to construct glassy polymers with room-temperature self-healing ability. This strategy relies on the unique molecular structure and multiple hydrogen bonds of RHP. The high density of the multiple hydrogen bonds imparts the RHP materials with T_g higher than room temperature and storage modulus up to 2.7 GPa at room temperature. The unique molecular structure of RHP not only endows the branching units and terminal groups with high mobility, but also prevents the ordered packing of molecular chains, which leads to the coexistence of the free and associated complementary moieties of hydrogen bonds. Due to the molecular mobility, the free complementary moieties can exchange with the associated moieties of hydrogen bonds, enabling reconfiguration of the dynamic network at room temperature. As a result, RHP manifests self-healing ability at 25 °C without the intervention of external stimuli, despite the glassy nature of the materials. In particular, the instantaneous self-healing within 1 min can lead to a recovered tensile strength of 5.5 MPa, which is superior to most existing self-healing materials. The elaborate design of hydrogen-bonding complementary moieties in RHP is quite general. Such strategy can be easily extended to other dynamic bonds and branched polymers, leading to a generation of glassy polymers with room-temperature self-healing ability.

Materials and Methods

In brief, we synthesized a series of RHP by one-pot Michael addition between MBA and BDA. The RHP films were made by hot press at 100 °C. Additional details of experimental materials and methods are provided in *SI Appendix*.

Data and Materials Availability. All data and materials needed to evaluate the conclusions in the paper are present in the paper, *SI Appendix* and Movie S1.

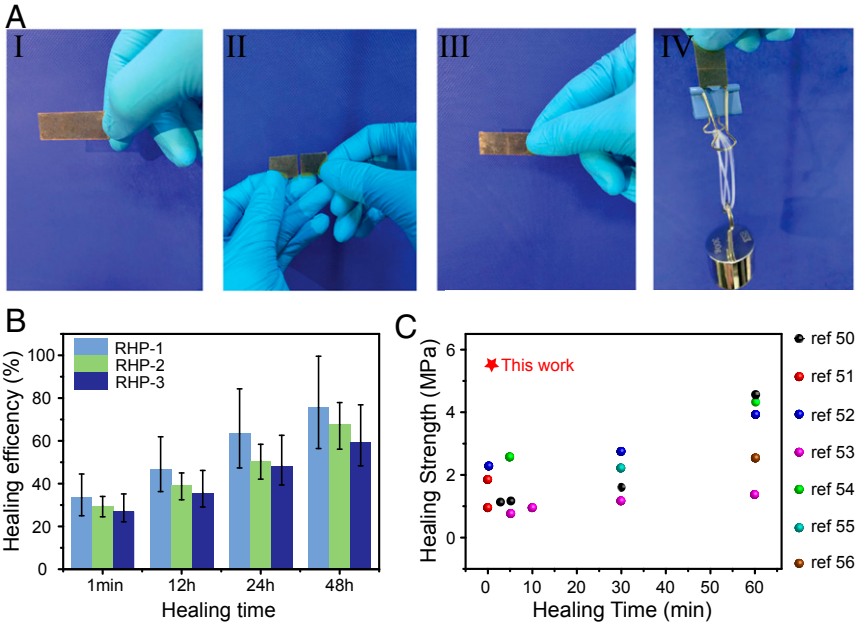

Fig. 5. Self-healing properties of RHP. (*A*) Photographs demonstrating the instantaneous healing of RHP-1: I) the original state of RHP-1, II) the state after being cut, III) the healed state after 1 min, IV) followed by bearing a weight of 300 g. (*B*) Healing efficiency of the RHP samples healed at 25 °C for different time periods. (*C*) Comparison of instantaneous self-healing strength (healing time less than 60 min) at room temperature among different self-healing materials with our work (50–56).

ACKNOWLEDGMENTS. This work was supported by National Natural Science Foundation of China (Grants 51873110 and 51673120), State Key Laboratory of Polymer Materials Engineering (Grant sklpme2019-2-14), and the Fundamental Research Funds for Central Universities.

1. Y. Chen, A. M. Kushner, G. A. Williams, Z. Guan, Multiphase design of autonomic self-healing thermoplastic elastomers. *Nat. Chem.* **4**, 467–472 (2012).
2. J. F. Patrick, M. J. Robb, N. R. Sottos, J. S. Moore, S. R. White, Polymers with autonomous life-cycle control. *Nature* **540**, 363–370 (2016).
3. Y. Yang, M. W. Urban, Self-healing polymeric materials. *Chem. Soc. Rev.* **42**, 7446–7467 (2013).
4. J. L. Wietor, R. P. Sijbesma, A self-healing elastomer. *Angew. Chem. Int. Ed. Engl.* **47**, 8161–8163 (2008).
5. M. D. Hager, P. Greil, C. Leyens, S. van der Zwaag, U. S. Schubert, Self-healing materials. *Adv. Mater.* **22**, 5424–5430 (2010).
6. X. Chen *et al.*, A thermally re-mendable cross-linked polymeric material. *Science* **295**, 1698–1702 (2002).
7. P. Cordier, F. Tournilhac, C. Soulié-Ziakovic, L. Leibler, Self-healing and thermoreversible rubber from supramolecular assembly. *Nature* **451**, 977–980 (2008).
8. D. Montarnal, M. Capelot, F. Tournilhac, L. Leibler, Silica-like malleable materials from permanent organic networks. *Science* **334**, 965–968 (2011).
9. S. R. White *et al.*, Autonomic healing of polymer composites. *Nature* **409**, 794–797 (2001).
10. K. S. Toohey, N. R. Sottos, J. A. Lewis, J. S. Moore, S. R. White, Self-healing materials with microvascular networks. *Nat. Mater.* **6**, 581–585 (2007).
11. M. Liu *et al.*, Supramolecular silicone coating capable of strong substrate bonding, readily damage healing, and easy oil sliding. *Sci. Adv.* **5**, eaaw5643 (2019).
12. J. Wu, L. H. Cai, D. A. Weitz, Tough self-healing elastomers by molecular enforced integration of covalent and reversible networks. *Adv. Mater.* **29**, 1702616 (2017).
13. S. Yoshida, H. Ejima, N. Yoshie, Tough elastomers with superior self-recoverability induced by bioinspired multiphase design. *Adv. Funct. Mater.* **27**, 1701670 (2017).
14. J. Liu *et al.*, Tough supramolecular polymer networks with extreme stretchability and fast room-temperature self-healing. *Adv. Mater.* **29**, 1605325 (2017).
15. J. Liu *et al.*, Biomimetic supramolecular polymer networks exhibiting both toughness and self-recovery. *Adv. Mater.* **29**, 1604951 (2017).
16. G. Weng, S. Thanneeru, J. He, Dynamic coordination of Eu-iminodiacetate to control fluorochromic response of polymer hydrogels to multistimuli. *Adv. Mater.* **30**, 1706526 (2018).
17. J. Y. Oh *et al.*, Stretchable self-healable semiconducting polymer film for active-matrix strain-sensing array. *Sci. Adv.* **5**, eaav3097 (2019).
18. N. Huebsch *et al.*, Ultrasound-triggered disruption and self-healing of reversibly cross-linked hydrogels for drug delivery and enhanced chemotherapy. *Proc. Natl. Acad. Sci. U.S.A.* **111**, 9762–9767 (2014).
19. C.-H. Li *et al.*, A highly stretchable autonomous self-healing elastomer. *Nat. Chem.* **8**, 618–624 (2016).
20. Y. Peng *et al.*, Super tough and strong self-healing elastomers based on polyampholytes. *J. Mater. Chem. A* **6**, 19066–19074 (2018).
21. F. Luo *et al.*, Oppositely charged polyelectrolytes form tough, self-healing, and rebuildable hydrogels. *Adv. Mater.* **27**, 2722–2727 (2015).
22. A. Das *et al.*, Ionic modification turns commercial rubber into a self-healing material. *ACS Appl. Mater. Interfaces* **7**, 20623–20630 (2015).
23. G. Du *et al.*, Nacre-mimetic composite with intrinsic self-healing and shape-programming capability. *Nat. Commun.* **10**, 800 (2019).
24. P. Taynton *et al.*, Heat- or water-driven malleability in a highly recyclable covalent network polymer. *Adv. Mater.* **26**, 3938–3942 (2014).
25. Z. Zou *et al.*, Rehealable, fully recyclable, and malleable electronic skin enabled by dynamic covalent thermoset nanocomposite. *Sci. Adv.* **4**, eaaq0508 (2018).
26. T. Oku, Y. Furusho, T. Takata, A concept for recyclable cross-linked polymers: Topologically networked polyrotaxane capable of undergoing reversible assembly and disassembly. *Angew. Chem. Int. Ed. Engl.* **43**, 966–969 (2004).
27. A. Rekondo *et al.*, Catalyst-free room-temperature self-healing elastomers based on aromatic disulfide metathesis. *Mater. Horiz.* **1**, 237–240 (2014).
28. H. Ying, Y. Zhang, J. Cheng, Dynamic urea bond for the design of reversible and self-healing polymers. *Nat. Commun.* **5**, 3218 (2014).
29. O. R. Cromwell, J. Chung, Z. Guan, Malleable and self-healing covalent polymer networks through tunable dynamic boronic ester bonds. *J. Am. Chem. Soc.* **137**, 6492–6495 (2015).
30. Y. Chen, Z. Tang, Y. Liu, S. Wu, B. Guo, Mechanically robust, self-healable, and reprocessable elastomers enabled by dynamic dual cross-links. *Macromolecules* **52**, 3805–3812 (2019).
31. J. J. Cash, T. Kubo, A. P. Bapat, B. S. Sumerlin, Room-temperature self-healing polymers based on dynamic-covalent boronic esters. *Macromolecules* **48**, 2098–2106 (2015).
32. I. Jeon, J. Cui, W. R. Illeperuma, J. Aizenberg, J. J. Vlassak, Extremely stretchable and fast self-healing hydrogels. *Adv. Mater.* **28**, 4678–4683 (2016).
33. Y. Zhang *et al.*, Malleable and recyclable poly (urea-urethane) thermosets bearing hindered urea bonds. *Adv. Mater.* **28**, 7646–7651 (2016).
34. Y. Ce, M. Q. Zhang, M. Z. Rong, Application of alkoxyamine in self-healing of epoxy. *J. Mater. Chem. A* **2**, 6558–6566 (2014).
35. C. Bao, Z. Guo, H. Sun, J. Sun, Nitrogen-coordinated boroxines enable the fabrication of mechanically robust supramolecular thermosets capable of healing and recycling under mild conditions. *ACS Appl. Mater. Interfaces* **11**, 9478–9486 (2019).
36. Y. Cao *et al.*, Self-healing electronic skins for aquatic environments. *Nat. Electron.* **2**, 75–82 (2019).
37. Y. Yanagisawa, Y. Nan, K. Okuro, T. Aida, Mechanically robust, readily repairable polymers via tailored noncovalent cross-linking. *Science* **359**, 72–76 (2018).
38. J. Mijović, S. Ristić, J. Kenny, Dynamics of six generations of PAMAM dendrimers as studied by dielectric relaxation spectroscopy. *Macromolecules* **40**, 5212–5221 (2007).
39. J. Issberner, R. Moors, F. Vögtle, Dendrimers: From generations and functional groups to functions. *Angew. Chem. Int. Ed. Engl.* **33**, 2413–2420 (1995).

40. D. Yan, J. Hou, X. Zhu, J. J. Kosman, H. S. Wu, A new approach to control crystallinity of resulting polymers: Self-condensing ring opening polymerization. *Macromol. Rapid Commun.* **21**, 557–561 (2000).
41. C. Calcagno, C. Mariani, S. Teixeira, R. Mauler, The role of the MMT on the morphology and mechanical properties of the PP/PET blends. *Compos. Sci. Technol.* **68**, 2193–2200 (2008).
42. B. X. Yang, K. P. Pramoda, G. Q. Xu, S. H. Goh, Mechanical reinforcement of polyethylene using polyethylene-grafted multiwalled carbon nanotubes. *Adv. Funct. Mater.* **17**, 2062–2069 (2007).
43. A. Mulliken, M. Boyce, Mechanics of the rate-dependent elastic–plastic deformation of glassy polymers from low to high strain rates. *Int. J. Solids Struct.* **43**, 1331–1356 (2006).
44. M. Sun, S. Pejanović, J. Mijović, Dynamics of deoxyribonucleic acid solutions as studied by dielectric relaxation spectroscopy and dynamic mechanical spectroscopy. *Macromolecules* **38**, 9854–9864 (2005).
45. J. Cao *et al*., Multiple hydrogen bonding enables the self-healing of sensors for human-machine interactions. *Angew. Chem. Int. Ed. Engl.* **56**, 8795–8800 (2017).
46. Y. Song, Y. Liu, T. Qi, G. L. Li, Towards dynamic but supertough healable polymers through biomimetic hierarchical hydrogen-bonding interactions. *Angew. Chem. Int. Ed. Engl.* **57**, 13838–13842 (2018).
47. B. Sun, Y. Lin, P. Wu, H. W. Siesler, A FTIR and 2D-IR spectroscopic study on the microdynamics phase separation mechanism of the poly (N-isopropylacrylamide) aqueous solution. *Macromolecules* **41**, 1512–1520 (2008).
48. D. J. Skrovanek, S. E. Howe, P. C. Painter, M. M. Coleman, Hydrogen bonding in polymers: Infrared temperature studies of an amorphous polyamide. *Macromolecules* **18**, 1676–1683 (1985).
49. A. W. Bosman *et al*., Concerning the localization of end groups in dendrimers. *J. Am. Chem. Soc.* **120**, 8547–8548 (1998).
50. S. M. Kim *et al*., Superior toughness and fast self-healing at room temperature engineered by transparent elastomers. *Adv. Mater.* **30**, 1705145 (2018).
51. L. Zhang *et al*., A highly efficient self-healing elastomer with unprecedented mechanical properties. *Adv. Mater.* **31**, e1901402 (2019).
52. W. Guo *et al*., Plant oil and amino acid-derived elastomers with rapid room temperature self-healing ability. *J. Mater. Chem. A* **7**, 21927–21933 (2019).
53. Y. Pan, J. Hu, Z. Yang, L. Tan, From fragile plastic to room-temperature self-healing elastomer: Tuning quadruple hydrogen bonding interaction through one-pot synthesis. *ACS Appl. Polym. Mater.* **1**, 425–436 (2019).
54. H. Wang *et al*., Synthesis of self-healing polymers by scandium-catalyzed copolymerization of ethylene and anisylpropylenes. *J. Am. Chem. Soc.* **141**, 3249–3257 (2019).
55. J. Xu *et al*., Extremely stretchable, self-healable elastomers with tunable mechanical properties: Synthesis and applications. *Chem. Mater.* **30**, 6026–6039 (2018).
56. J.-C. Lai *et al*., Thermodynamically stable whilst kinetically labile coordination bonds lead to strong and tough self-healing polymers. *Nat. Commun.* **10**, 1164 (2019).